Chemical Science

ROYAL SOCIETY OF CHEMISTRY

EDGE ARTICLE

View Article Online
View Journal

Cite this: DOI: 10.1039/d6sc00060f

All publication charges for this article have been paid for by the Royal Society of Chemistry

Visible-light-driven valorization of 5-hydroxymethylfurfural over a hollow Co_3O_4@$Zn_3In_2S_6$ nanocage in base-free water under an air atmosphere

Rong Dang,[a] Kexin Fan,[a] Yan-Ning Wang,[b] Guangsheng Zhu,[a] Liu Liu,[c] Zifu Hu,[a] Taolian Guo,*[a] Wu Chen*[a] and Fengxiang Chen*[a]

Received 5th January 2026
Accepted 20th February 2026

DOI: 10.1039/d6sc00060f

rsc.li/chemical-science

Visible-light-driven upgrading of biomass-derived 5-hydroxymethylfurfural (5-HMF) represents a green and sustainable strategy. However, photocatalytic selective oxidation of HMF to generate 2,5-diformylfuran (DFF), a highly promising biomass-derived molecule for pharmaceuticals and heterocyclic ligands, is extremely challenging under green and mild conditions. Herein, we construct a hollow Co_3O_4@$Zn_3In_2S_6$ (ZC–x) nanocage photocatalyst, which exhibits a remarkable photocatalytic activity for the oxidation of HMF to DFF in base-free water under an air atmosphere. The optimal ZC-5 heterojunction achieves 95.4% HMF conversion and 94.1% DFF selectivity. The superior photocatalytic performance of the ZC-5 heterojunction is attributed to intimate interfacial contact between Co_3O_4 and $Zn_3In_2S_6$, which is beneficial to generate strong interfacial interaction and facilitate the separation of electron–hole pairs. Characteristic analysis and density functional theory (DFT) calculations elucidate that the enhanced built-in electric field (IEF) and S-scheme charge transfer mechanism within the ZC heterojunction effectively drive the selective photo-oxidation of HMF to DFF. This work offers an efficient strategy to design heterojunction photocatalysts for highly effective oxidation of HMF under mild conditions.

Introduction

Photocatalytic upgrading of renewable biomass resources is a prospective avenue to produce high value-added chemicals and simultaneously relieve the energy crisis and environmental pollution.[1–4] As an essential biomass-derived platform molecule, 5-hydroxymethylfurfural (HMF) can be converted into multiple value-added products due to its different functional groups including the alcohol hydroxyl group (–CH_2OH) and aldehyde group (–CHO).[5–8] In particular, 2,5-diformylfuran (DFF) generated by selective oxidation of HMF has been extensively utilized as a highly promising intermediate for synthesizing pharmaceuticals, resin and heterocyclic ligands.[9,10] However, the highly selective oxidation of –CH_2OH to produce DFF is extremely challenging during the photocatalytic HMF oxidation process, in which the appropriate oxidation capacity of photocatalysts is vital to avoid excessive oxidation.[11–13] Therefore, it is crucial to design effective photocatalysts for highly selective oxidation of HMF to DFF.

Transition metal sulfides, such as 2D layered $Zn_3In_2S_6$, an n-type semiconductor, have attracted widespread attention for the selective oxidation of HMF to DFF due to its suitable band energy and outstanding visible-light-responsive capability.[14] Based on the $Zn_3In_2S_6$ semiconductor, many efforts (morphology engineering, heteroatom doping, defect engineering, and heterostructure construction) have been adopted to further improve its photocatalytic efficiency.[15–19] Among them, the construction of the $Zn_3In_2S_6$-based heterostructure has been proven to be an efficient strategy for facilitating charge carrier separation, regulating the photoelectric characteristics, and integrating the advantages of different components, eventually improving photocatalytic performance.[20,21] Recently, the step scheme (S-scheme) heterojunction has emerged as an effective heterojunction system to achieve efficient electron–hole separation and retains their high redox capacities in semiconductor-based photocatalysts.[22–25] Specifically, the S-scheme heterojunction based on a p–n heterojunction system favors the formation of a strong built-in electric field (IEF), significantly improving photocatalytic activity.[26,27] As a typical p-type semiconductor photocatalyst, Co_3O_4 has aroused wide concern due to its non-poison, low cost, and tunable structural features.[28–30] Accordingly, integrating $Zn_3In_2S_6$ and Co_3O_4 to develop a heterojunction composite maybe indeed an effective approach for highly efficient photocatalytic oxidation of HMF into DFF.

[a]National Local Joint Engineering Laboratory for Advanced Textile Processing and Clean Production, and State Key Laboratory of New Textile Materials and Advanced Processing, Wuhan Textile University, Wuhan 430200, China. E-mail: tlguo@wtu.edu.cn; wuchen@wtu.edu.cn; fxchen_czx@wtu.edu.cn

[b]College of Chemistry and Chemical Engineering, Xinyang Normal University, Xinyang, Henan 464000, China

[c]Analytical and Testing Center, Wuhan Textile University, Wuhan 430200, China

In this work, we constructed a hollow Co_3O_4@$Zn_3In_2S_6$ (ZC) heterojunction by uniformly coating $Zn_3In_2S_6$ nanosheets (NSs) on the surface of ZIF-67-derived hollow Co_3O_4 nanocages for selective photo-oxidation of HMF to DFF.[31] The hollow architecture of Co_3O_4 nanocages afford large surface area to form intimate interfacial contact with $Zn_3In_2S_6$ NSs, which is beneficial to form strong interfacial interaction and facilitate the effective separation of electron–hole pairs. The optimal ZC-5 heterojunction delivers a remarkable HMF conversion rate of 95.4% with 94.1% DFF selectivity and a high yield of DFF (66.8%) under visible light irradiation and an air atmosphere in base-free water. Accordingly, characteristic analysis and density functional theory (DFT) calculations elucidate the charge transfer mechanism of S-scheme heterojunctions and the enhanced IEF effect, which improved interfacial charge separation and facilitated selective photo-oxidation of HMF to DFF. Moreover, a possible reaction mechanism for photocatalytic oxidation of HMF over the ZC S-scheme heterojunction has also been proposed. This work provides inspiring ideas to design heterojunction photocatalysts for upgrading biomass feedstock into higher-value chemicals under green and mild conditions.

Results and discussion

The synthetic process of the ZC–*x* S-scheme heterojunction is schematically illustrated in Fig. 1a. The high-quality Co_3O_4 nanocages were synthesized *via* the thermal treatment of ZIF-67 polyhedral precursors.[32] Afterward, the hierarchical ZC heterostructure was constructed by *in situ* growing $Zn_3In_2S_6$ NSs on the surface of the Co_3O_4 nanocages. The characteristic ZIF-67 peaks in the X-ray diffraction (XRD) pattern confirm its successful synthesis with a high degree of crystallinity (Fig. S1).[33] As illustrated in Fig. 1b and S2, the derived Co_3O_4 displays distinct diffraction peaks at 2θ = 31.4°, 36.8°, 45°, 59.5°, and 65.3°, corresponding to the (220), (311), (400), (511), and (440) lattice planes of the spinel structure of Co_3O_4 (PDF#43-1003), respectively.[31] The diffraction peaks of $Zn_3In_2S_6$ observed at 20.7°, 28.4°, 47.2°, and 56.2° can be attributed to the (005), (102), (110), and (203) crystalline planes of hexagonal $Zn_3In_2S_6$ (PDF#24-1453).[34] Obviously, the ZC samples exhibit characteristic diffraction peaks of both Co_3O_4 and $Zn_3In_2S_6$, and no impurity peaks were observed, further validating the successful synthesis of the highly crystalline ZC heterojunction.

X-ray photoelectron spectroscopy (XPS) was further measured to analyze the surface chemical compositions and states of the samples. The ZC-5 composite displays the presence of Co, O, S, Zn and In elements (Fig. S3). In the high-resolution O 1s spectrum of Co_3O_4, the peaks at approximately 529.91 eV, 531.16 eV, and 532.22 eV are corresponding to lattice oxygen (O_L), oxygen vacancies (O_v), and hydroxyl species (O–H), respectively (Fig. 1c).[31] For ZC-5, the corresponding peaks of O 1s shift to higher binding energies compared with those of individual Co_3O_4. In contrast, the peaks of S 2p, Zn 2p, and In 3d in ZC-5 shift toward the lower binding energy region

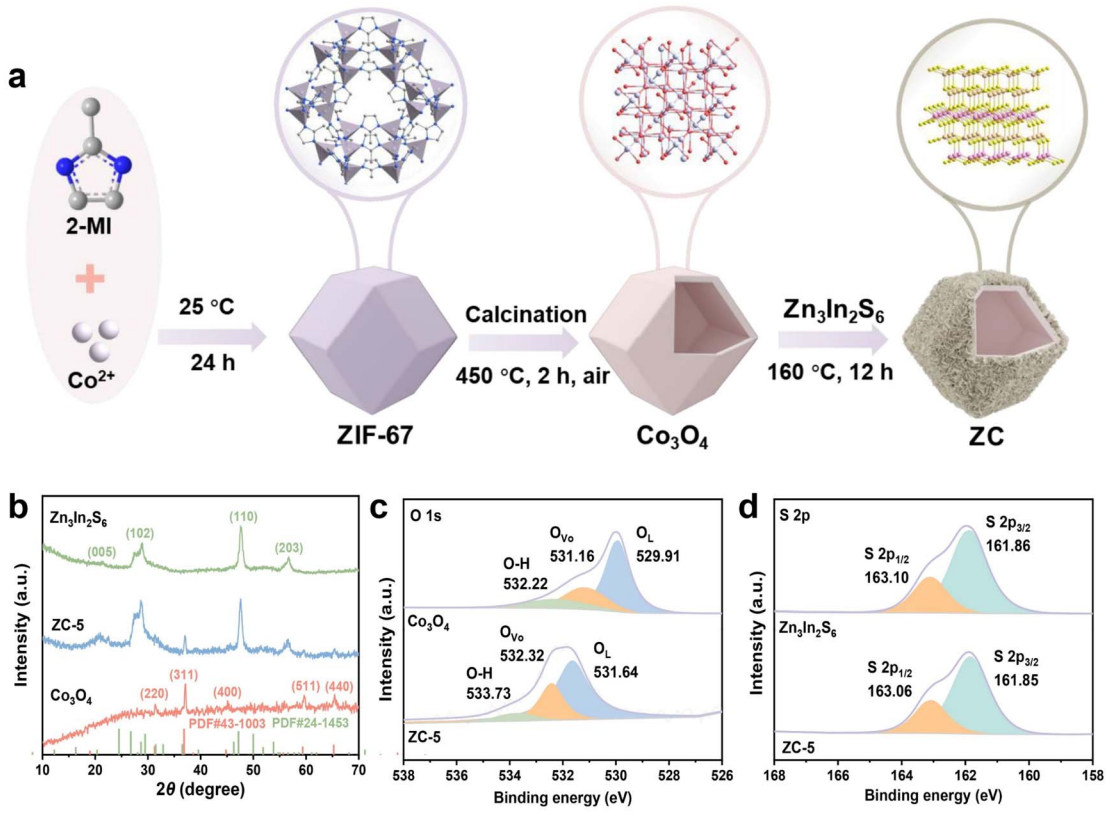

Fig. 1 (a) Schematic illustration of the preparation process of ZC. (b) XRD patterns of Co_3O_4, $Zn_3In_2S_6$, and ZC-5. (c) O 1s and (d) S 2p XPS spectra of Co_3O_4, $Zn_3In_2S_6$, and ZC-5.

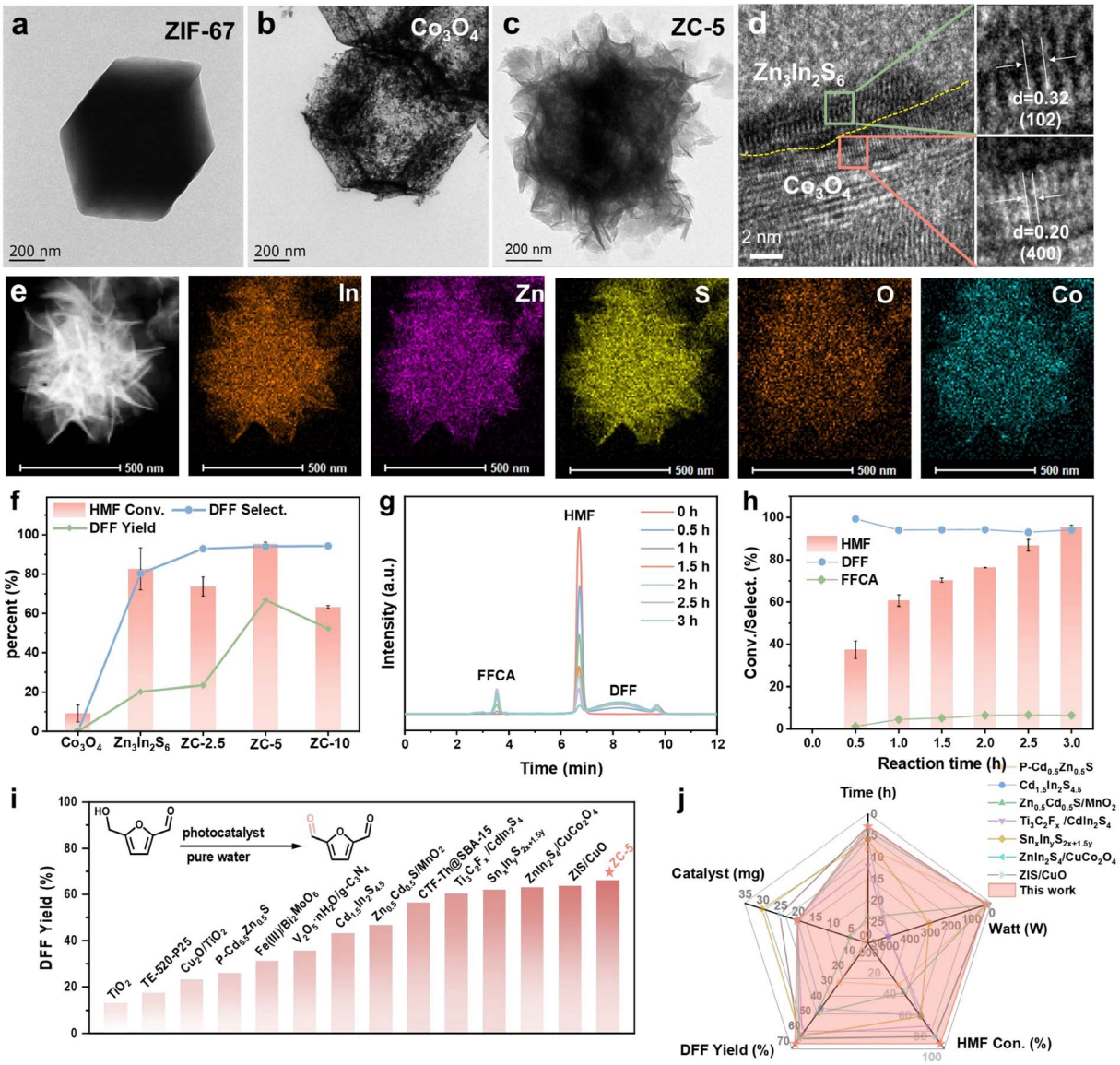

Fig. 2 (a–c) TEM images of ZIF-67, Co_3O_4, and ZC-5. (d) HRTEM and (e) elemental mapping images of ZC-5. (f) Photocatalytic oxidation of HMF into DFF over different photocatalysts. (g) Time-dependent monitoring of HPLC in HMF oxidation over 3 h. (h) Time-dependent conversion of HMF into DFF over ZC-5. (i) Comparison of DFF yield with reported studies. (j) Comparison of the photo-oxidation performance of HMF with reported photocatalysts.

compared with pure $Zn_3In_2S_6$ (Fig. 1d, S4a and b).[35–37] The peaks of Co 2p are difficult to observe due to their low surface content (Fig. S4c).[33] The shifts of binding energies imply the occurrence of charge transfer within the ZC-5 heterojunction, confirming the formation of a strong interaction between Co_3O_4 and $Zn_3In_2S_6$.

Scanning electron microscopy (SEM) and transmission electron microscopy (TEM) were performed to characterize the microstructures of as-prepared materials. ZIF-67 exhibits a dodecahedral morphology with a diameter of approximately 2 μm (Fig. 2a and S5). After calcination, Co_3O_4 was presented in the form of a hollow nanocage (Fig. 2b and S6). $Zn_3In_2S_6$ exhibits a micro-flowerlike structure consisting of multiple nanosheets (Fig. S7). When $Zn_3In_2S_6$ was *in situ* assembled on the surface of hollow Co_3O_4 nanocages, $Zn_3In_2S_6$ NSs were uniformly and closely covered on Co_3O_4 nanocages (Fig. 2c and S8). The high-resolution TEM (HRTEM) images (Fig. 2d) of ZC-5 demonstrate an intimate interfacial contact between $Zn_3In_2S_6$ and Co_3O_4, which can effectively promote the charge carrier transport. The lattice fringes observed at 0.20 and 0.32 nm are ascribed to the (400) plane of Co_3O_4 and the (102) plane of $Zn_3In_2S_6$, respectively.[38–40] Elemental mapping images indicate the presence of Co, O, S, Zn, and In elements within ZC-5, where S, Zn and In elements are uniformly distributed over the whole surface of Co_3O_4 (Fig. 2e). In addition, nitrogen adsorption–desorption measurements were conducted to analyse the porosity structure of these samples (Fig. S9 and Table S1). The ZC-5 heterojunction presents both the microporous structure of

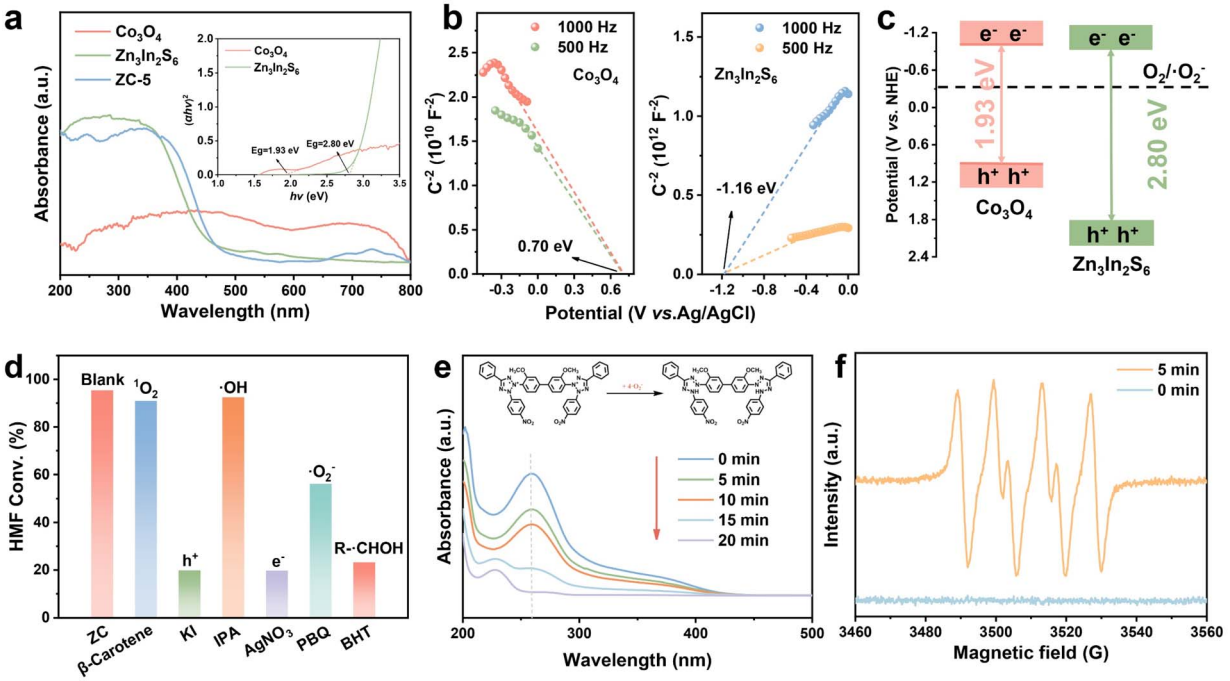

Fig. 3 (a) UV-vis DRS spectra and Tauc plots of Co_3O_4, $Zn_3In_2S_6$, and ZC. (b) Mott–Schottky plots of Co_3O_4 and $Zn_3In_2S_6$. (c) The band structures of Co_3O_4 and $Zn_3In_2S_6$. (d) HMF conversion rates with the addition of various scavengers during the photocatalytic HMF oxidation over the ZC-5 heterojunction. (e) UV-vis absorbance spectra of NBT degradation over ZC-5. (f) EPR spectra of $^{\bullet}O_2^-$ generated before and after light irradiation for 5 min.

Co_3O_4 and the mesoporous feature of $Zn_3In_2S_6$, which are advantageous for exposing more active sites.

Furthermore, the photocatalytic performance of the catalysts for HMF oxidation was evaluated under visible-light irradiation in base-free water and atmospheric oxygen. As shown in Fig. 2f, pure $Zn_3In_2S_6$ exhibits a high HMF conversion rate of 82.7%, yet the yield of DFF is only 20.2%. When Co_3O_4 was alone used as the photocatalyst, minimal activity was displayed and no DFF was detected. Excitingly, the ZC heterojunctions enhanced catalytic activity and significantly improved the yield of DFF. The ZC heterojunctions with varying amounts of Co_3O_4 show distinct activity in the photocatalytic oxidation of HMF. Notably, ZC-5 with the optimal proportion (5% Co_3O_4) demonstrated exceptional performance, achieving 95.4% conversion of HMF with a 94.1% DFF selectivity and only trace amounts of FFCA detected as a byproduct (Fig. 2g, h and S10). More importantly, the yield of DFF (66.8%) was increased to three times that over $Zn_3In_2S_6$, surpassing most reported photocatalysts under aqueous conditions (Fig. 2i and Table S3). In summary, the systematic comparison of HMF conversion rate, DFF yield, reaction time, catalyst amount and lamp power is presented in Fig. 2j, and ZC-5 exhibits superior photocatalytic performance compared to all control samples. Besides, the activity of ZC-5 showed almost no attenuation after five cycles, indicating excellent photocatalytic stability (Fig. S11), which was further verified by the XRD and XPS analyses of the used catalyst (Fig. S12 and S13).

UV-vis diffuse reflectance spectroscopy (DRS, Fig. 3a) was used to investigate the optical properties and band structures of the samples, which is critical for selective photocatalytic oxidation of HMF. The ZIF-67-derived Co_3O_4 exhibits superior visible-light response capacity, which is ascribed to its rough, porous morphology and high surface area inherited from ZIF-67, promoting light scattering and internal reflection.[41,42] Compared with pristine $Zn_3In_2S_6$, the ZC composite shows obviously enhanced visible-light absorption after incorporation of Co_3O_4. The band gap energies (E_g) of Co_3O_4 and $Zn_3In_2S_6$ were calculated to be 1.93 and 2.80 eV, respectively, which were determined from the corresponding Tauc plots (Fig. 3a inset).[43] The Mott–Schottky (M–S) analysis indicates that $Zn_3In_2S_6$ is an n-type semiconductor, while Co_3O_4 is a p-type semiconductor (Fig. 3b).[31,44] The flat-band potentials E_{fb} of Co_3O_4 and $Zn_3In_2S_6$ were 0.70 and −1.16 eV based on the M–S plots. Accordingly, the valence band (VB) of Co_3O_4 is 0.92 eV and the conduction band (CB) of $Zn_3In_2S_6$ is −0.94 eV, respectively, which were adjusted to account for the standard redox potential (0.22 eV) of the Ag/AgCl electrode.[11,12] Hence, the calculated E_{CB} of Co_3O_4 is −1.01 eV and the E_{VB} of $Zn_3In_2S_6$ is 1.86 eV. The above results demonstrate that the ZC heterojunction exhibits a suitable band structure for the photocatalytic oxidation of HMF (Fig. 3c).

To elucidate the photo-oxidation mechanism of HMF, scavenger tests were conducted through adding different quenchers.[45] The roles of electron–hole pairs and reactive oxygen species (ROS) during the photocatalytic HMF oxidation over the ZC-5 heterojunction are illustrated in Fig. 3d. With the addition of KI and $AgNO_3$ (h^+ and e^- quenchers, respectively), the conversion rate of HMF (19.8% and 19.7%) was significantly decreased.[36,46] β-Carotene and isopropanol (IPA) were added to

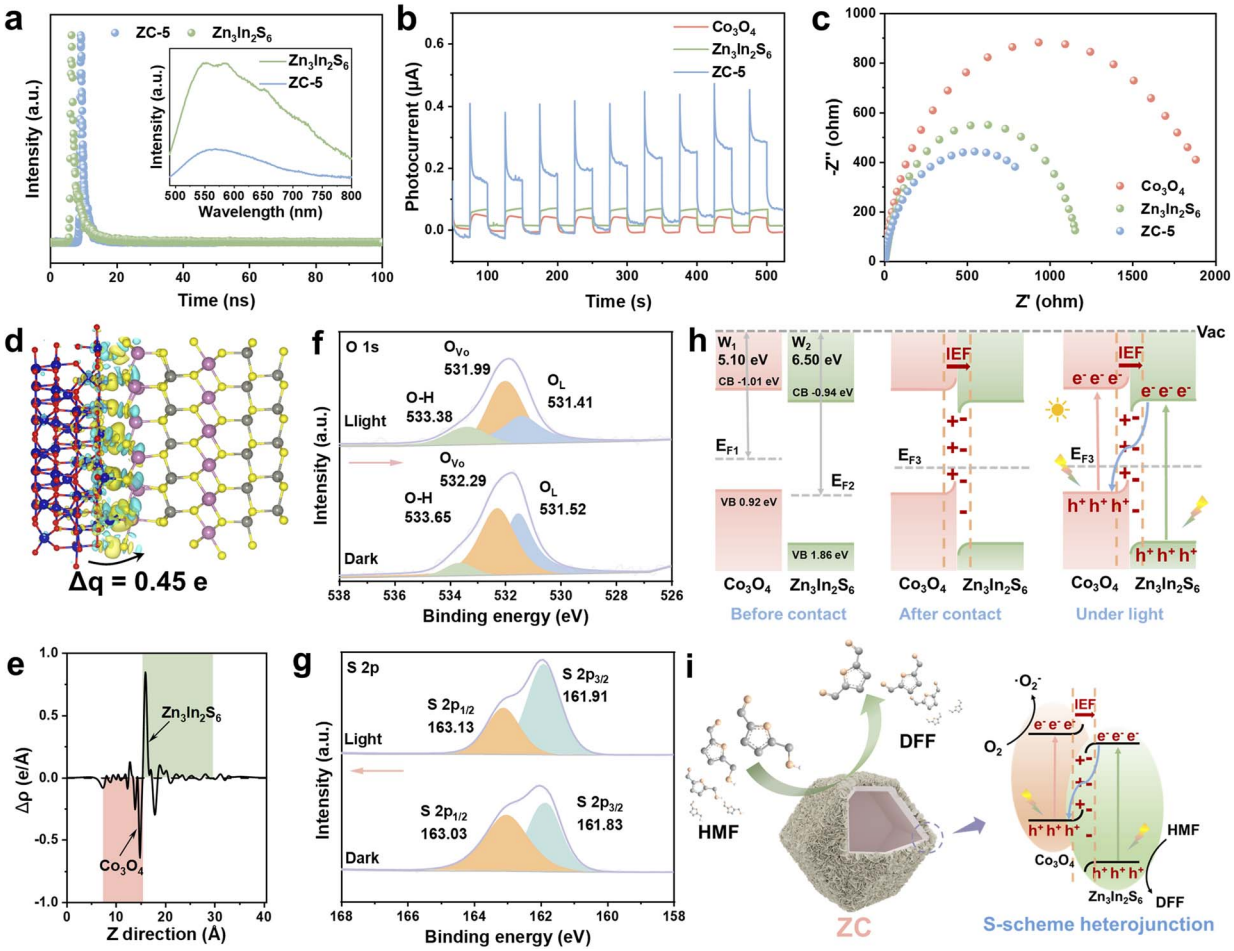

Fig. 4 (a) PL spectra and fluorescence life time spectra of $Zn_3In_2S_6$ and ZC-5. (b) Transient photocurrent curves and (c) electrochemical impedance spectra of Co_3O_4, $Zn_3In_2S_6$ and ZC-5. (d) Calculated charge density difference for the ZC heterostructure. (e) Planar averaged electron density difference for ZC (the green and pink areas indicate electron accumulation and depletion, respectively). *In situ* XPS spectra of (f) O 1s and (g) S 2p for ZC-5 under light irradiation. (h) Possible charge migration and separation mechanism of the ZC S-scheme heterojunction. (i) Illustration showing the photo-oxidation of HMF to DFF over ZC.

inhibit the generation of $^1O_2$ and $^{\cdot}OH$, respectively, and resulted in a negligible variation in the conversion rate. When PBQ was added into the photocatalytic system, the HMF conversion rate was also reduced from 95.4% to 56.2%, suggesting that $^{\cdot}O_2^-$ is the dominant ROS in the photo-oxidation of HMF over the ZC-5 heterojunction. Besides, the addition of 6-di-*tert*-butyl-4-methylphenol (BHT) can inhibit the generation of the R-$^{\cdot}$CHOH radical and results in the reduction of HMF conversion, suggesting that R-CH_2OH is oxidized by h^+ to produce the R-$^{\cdot}$CHOH radical during the photocatalytic oxidation process of HMF to DFF. Nitroblue tetrazolium (NBT) was further utilized as a probe to evaluate the ability of ZC-5 to generate $^{\cdot}O_2^-$.[47,48] As shown in Fig. 3e and S14, upon irradiation, the conversion rate of NBT by the ZC-5 photocatalyst can reach 100% within 20 min, demonstrating that $^{\cdot}O_2^-$ plays a crucial role in the catalytic process. Compared with Co_3O_4 and $Zn_3In_2S_6$, the higher NBT degradation rate of ZC-5 demonstrates the enhanced generation of $^{\cdot}O_2^-$, thus promoting photocatalytic oxidation of HMF. Electron paramagnetic resonance (EPR) measurements were also performed using 5,5-dimethyl-1-pyrroline N-oxide (DMPO) as a trapping agent to accurately identify the generation of $^{\cdot}O_2^-$ by the ZC-5 heterojunction. The distinct DMPO-$^{\cdot}O_2^-$ signals were detected upon irradiation, whereas no signals were detected without light irradiation (Fig. 3f).[49] These findings illustrate the main ROS ($^{\cdot}O_2^-$) and the formation pathway (R-$^{\cdot}$CHOH) in the photocatalytic conversion of HMF to DFF.

The efficiency of photogenerated carrier separation and migration is vitally important for achieving high photocatalytic performance. To elucidate the charge transfer kinetics on the ZC catalyst, photoluminescence (PL) and photo/electrochemical measurements were conducted. As shown in Fig. 4a, the ZC-5 composite exhibits significantly weaker photoluminescence (PL) intensity than that of $Zn_3In_2S_6$, indicating that the construction of the ZC S-scheme heterojunction can inhibit charge recombination.[33,50] In addition, the time-resolved photoluminescence (TR-PL) decay spectra display that the average fluorescence lifetime of ZC-5 (1.42 ns) is shorter than that of $Zn_3In_2S_6$ (3.13 ns), demonstrating that the construction of the

heterojunction significantly suppresses the recombination of photogenerated e^--h^+ pairs (Fig. 4a and Table S2). The transient photocurrent curve (Fig. 4b) reveals that the ZC-5 heterojunction displays much higher photocurrent density than Co_3O_4 and $Zn_3In_2S_6$, indicating that the ZC S-scheme heterojunction can efficiently facilitate the separation and transport of photogenerated charges. Furthermore, the electrochemical impedance spectroscopy (EIS, Fig. 4c) results show that ZC-5 exhibits a smaller semicircle and lower charge transfer resistance in the Nyquist plot compared to Co_3O_4 and $Zn_3In_2S_6$, and thus electrons in ZC-5 can migrate more readily, resulting in a faster transfer efficiency of photogenerated charge carriers.

Furthermore, density functional theory (DFT) calculations were conducted to comprehend the detailed interface interaction and charge transfer mechanism of the ZC composite. Upon the formation of the heterojunction, the potential difference between the surfaces of Co_3O_4 and $Zn_3In_2S_6$ facilitates the transport of free electrons, which can be reflected through work function determined by DFT calculation according to the equation $\Phi = E_{vac} - E_F$.[51,52] The work functions of Co_3O_4 and $Zn_3In_2S_6$ are 5.1 and 6.5 eV, respectively (Fig. S15). Since the E_F of Co_3O_4 is higher than that of $Zn_3In_2S_6$, electrons spontaneously migrate from high E_F (Co_3O_4) to low E_F ($Zn_3In_2S_6$) until the Fermi energy levels reach equilibrium, thereby establishing IEF.[53,54] As illustrated in Fig. 4d and e, the charge density difference (CDF) of ZC shows that electron transfer occurs in the interface between Co_3O_4 and $Zn_3In_2S_6$, where electrons accumulated on $Zn_3In_2S_6$ and depleted on Co_3O_4, respectively. The redistribution of electrons resulted in the establishment of IEF (Fig. 4h). Under light irradiation, the IEF induces the recombination of electrons in the CB of $Zn_3In_2S_6$ and holes in the VB of Co_3O_4, establishing an S-scheme electron transfer mechanism between Co_3O_4 and $Zn_3In_2S_6$. *In situ* XPS spectroscopy measurements were conducted to further explore the transfer direction of photogenerated electrons in the ZC heterojunction during the photocatalytic process. As shown in Fig. 4f, g and S16, the binding energy of O 1s shifts toward lower values under light irradiation, while those of S 2p, In 3d, and Zn 2p in ZC-5 shift toward higher values. These observations indicate that the IEF drives charge transfer across the heterojunction interface. Specifically, photoexcited electrons in the conduction band of $Zn_3In_2S_6$ are transferred to Co_3O_4 under the influence of the IEF, thereby promoting the formation of an S-scheme heterojunction within the ZC composite catalyst.

Based on the aforementioned characterization studies, the underlying mechanism for the improved photocatalytic performance of the ZC heterojunction for the oxidation of HMF to DFF is preliminarily proposed (Fig. 4i). Upon light illumination, the photoexcited $e^- - h^+$ pairs are generated at the first. Subsequently, the strong IEF within the ZC S-scheme heterojunction effectively drove the separation of photoexcited e^- and h^+ and facilitate their migration along the interface of $Zn_3In_2S_6$ and Co_3O_4. Owing to the S-scheme electron transfer mechanism of the ZC heterojunction, photogenerated e^- in the CB of $Zn_3In_2S_6$ and photogenerated h^+ in the VB of Co_3O_4 undergo recombination at the interface. Meanwhile, the photogenerated e^- retained in the CB of Co_3O_4 efficiently reduce O_2 to $^{\bullet}O_2^-$ radicals, while the photogenerated h^+ left in the VB of $Zn_3In_2S_6$ oxidize HMF to generate active intermediates, which then react with $^{\bullet}O_2^-$ to produce DFF.

Conclusions

In summary, we have successfully constructed a hollow Co_3O_4@$Zn_3In_2S_6$ nanocage photocatalyst for enhancing photooxidation of HMF to DFF under visible light irradiation and an air atmosphere in pure water. The intimate interfacial contact between Co_3O_4 and $Zn_3In_2S_6$ forms the strong interfacial interaction and accelerates the transfer of photogenerated charge carriers, resulting in remarkable photocatalytic performance. The optimal ZC-5 heterojunction achieves the highest HMF conversion rate (95.4%) and DFF selectivity (94.1%), as well as an increased DFF yield (66.8%). The systematic experiment analysis and DFT calculations elucidated that the formation of a strong IEF and an S-scheme charge transform mechanism within the ZC heterojunction can effectively drive the charge separation and migration, leading to enhanced photo-oxidation of HMF to DFF. This study provides an effective strategy for developing high-performance photocatalysts by designing a hollow nanocage heterojunction for oxidizing HMF to produce DFF under mild conditions.

Author contributions

Rong Dang: validation, methodology, investigation, formal analysis, writing – original draft. Kexin Fan: data curation. Yan-Ning Wang: data curation. Guangsheng Zhu: data curation. Liu Liu: data curation. Zifu Hu: data curation. Taolian Guo: writing – review & editing, validation, methodology, supervision, funding acquisition, conceptualization. Wu Chen: writing – review & editing, supervision. Fengxiang Chen: writing – review & editing, supervision, funding acquisition. All authors analyzed and discussed the experimental results.

Conflicts of interest

There are no conflicts to declare.

Data availability

The data supporting this article have been included as part of the supplementary information (SI). Supplementary information is available. See DOI: https://doi.org/10.1039/d6sc00060f.

Acknowledgements

This work was supported by grants from the National Natural Science Foundation of China (52373085, 52573090, U21A2095, and 52533017), Educational Commission of Hubei Province of China (Q20231711), Department of Science and Technology of Hubei Province (No. 2025CSA001 and 2024CSA076), Outstanding Young and Middle-aged Scientific and Technology Innovation Team of Higher Education Institutions of Hubei Province (No. T2024010), Innovative Team Program of Natural

Science Foundation of Hubei Province (No. 2023AFA027), and Major Fundamental Research of Natural Science Foundation of Shandong Province (ZR2025ZD33). We thank the Analytical and Testing Center of Wuhan Textile University for the HPLC tests. The authors acknowledge Jinan Gengzi Supercomputing Cloud Tech Co., Ltd. for providing High Performance Computing resources that support the theoretical calculations.

References

1 N. Li, K. Yan, T. Rukkijakan, J. Liang, Y. Liu, Z. Wang, H. Nie, S. Muangmeesri, G. Castiella-Ona, X. Pan, Q. Zhou, G. Jiang, G. Zhou, J. Ralph, J. S. M. Samec and F. Wang, *Nature*, 2024, **630**, 381–386.
2 F. Vidal, E. R. van der Marel, R. W. F. Kerr, C. McElroy, N. Schroeder, C. Mitchell, G. Rosetto, T. T. D. Chen, R. M. Bailey, C. Hepburn, C. Redgwell and C. K. Williams, *Nature*, 2024, **626**, 45–57.
3 Z. Huang, Z. Zhao, C. Zhang, J. Lu, H. Liu, N. Luo, J. Zhang and F. Wang, *Nat. Catal.*, 2020, **3**, 170–178.
4 D. Shi, J. Zhang, Z. Qi, L. Duan, R. Yu, Q. Yue, D. Meng, T. Kang, L. Liu, K. Lan, W. Li, D. Zhao, L. Wu and Y. Ma, *Adv. Mater.*, 2025, **37**, 2510246.
5 L. Chico-Mesa, A. Rodes, R. M. Arán-Ais and E. Herrero, *Nat. Commun.*, 2025, **16**, 3349.
6 X. Cao, Y. Ding, D. Chen, W. Ye, W. Yang and L. Sun, *J. Am. Chem. Soc.*, 2024, **146**, 25125–25136.
7 T. Xia, W. Gong, Y. Chen, M. Duan, J. Ma, X. Cui, Y. Dai, C. Gao and Y. Xiong, *Angew. Chem., Int. Ed.*, 2022, **61**, e202204225.
8 Z. Li, M. Zhang, X. Xin and H. Lv, *ChemCatChem*, 2021, **13**, 1389–1395.
9 W. Xue, J. Ye, Z. Zhu, R. Kumar and J. Zhao, *Energy Environ. Sci.*, 2025, **18**, 214–226.
10 Y. Gao, L. Ge, H. Xu, K. Davey, Y. Zheng and S.-Z. Qiao, *ACS Catal.*, 2023, **13**, 11204–11231.
11 Y. Liu, W. Xue, J. Ye, R. Zhang, Y. Shao, A. P. Rangappa and J. Zhao, *Chem. Eng. J.*, 2025, **515**, 163620.
12 M. Zhang, Z. Li, X. Xin, J. Zhang, Y. Feng and H. Lv, *ACS Catal.*, 2020, **10**, 14793–14800.
13 S. Jiang, Z. Chen, S. Xiong, H. Zhao, X. Xiao and Z. Shen, *J. Energy Chem.*, 2025, **109**, 830–838.
14 S. Xiong, X. Liu, Z. Shen, Z. Hu, H. Yang, J. Hao, J. Cai and J. Yang, *Inorg. Chem.*, 2023, **62**, 20120–20128.
15 D. Jiao, C. Ding, M. Xu, X. Ruan, S. K. Ravi and X. Cui, *Adv. Funct. Mater.*, 2024, **35**, 2416753.
16 J. Chen, M. Mu, Z. Wang, M. Ma, F. A. Qaraah, X. Yin and G. Bai, *ACS Sustainable Chem. Eng.*, 2024, **12**, 18161–18173.
17 T. Liu, Y. Xiong, X. Wang, Y. Xue, W. Liu and J. Tian, *J. Colloid Interface Sci.*, 2023, **640**, 31–40.
18 J. L. Zhou, Y. F. Mu, M. Qiao, M. R. Zhang, S. X. Yuan, M. Zhang and T. B. Lu, *Angew. Chem., Int. Ed.*, 2025, **64**, e202506963.
19 C. Li, X. Hu, Z. Chen and Z. Ding, *Sep. Purif. Technol.*, 2025, **377**, 134344.
20 Y. Che, K. Wang, C. Wang, B. Weng, S. Chen and S. Meng, *J. Mater. Sci. Technol.*, 2026, **243**, 228–236.
21 X. Ruan, S. Zhao, M. Xu, D. Jiao, J. Leng, G. Fang, D. Meng, Z. Jiang, S. Jin, X. Cui and S. K. Ravi, *Adv. Energy Mater.*, 2024, **14**, 2401744.
22 X. Tan, S. Si, D. Xiao, X. Bao, K. Song, Z. Wang, Y. Liu, Z. Zheng, P. Wang, Y. Dai, B. Huang and H. Cheng, *ACS Catal.*, 2023, **13**, 14395–14403.
23 S. Wan, W. Wang, B. Cheng, G. Luo, Q. Shen, J. Yu, J. Zhang, S. Cao and L. Zhang, *Nat. Commun.*, 2024, **15**, 9612.
24 X. Deng, J. Zhang, K. Qi, G. Liang, F. Xu and J. Yu, *Nat. Commun.*, 2024, **15**, 4807.
25 Q. P. Huang, C. Yang, Q. Yin, A. A. Zhang, H. X. Liu, L. Li, M. M. Liu, Z. B. Fang and T. F. Liu, *Angew. Chem., Int. Ed.*, 2025, **64**, e202502009.
26 K. Huang, G. Liang, S. Sun, H. Hu, X. Peng, R. Shen and X. Li, *J. Mater. Sci. Technol.*, 2024, **193**, 98–106.
27 L. Shi, Y. Wu, Z. Chang, P. Jiang, Y. Hua, Q. Shi, S. Hou and H. Wang, *Appl. Catal., B*, 2025, **378**, 125618.
28 L. Xu, Q. Jiang, Z. Xiao, X. Li, J. Huo, S. Wang and L. Dai, *Angew. Chem., Int. Ed.*, 2016, **55**, 5277–5281.
29 B. Yan, Q. Ruan, S. Wang, L. Kong, P. Zhang, H. Wang and Z. Sun, *Adv. Funct. Mater.*, 2024, **34**, 2408895.
30 S. Bai, W. Jing, G. He, C. Liao, F. Wang, Y. Liu and L. Guo, *ACS Nano*, 2023, **17**, 10976–10986.
31 J. Fan, L. Shi, H. Ge, J. Liu, X. Deng, Z. Li and Q. Liang, *Adv. Funct. Mater.*, 2024, **35**, 2412078.
32 D. Ding, K. Shen, X. Chen, H. Chen, J. Chen, T. Fan, R. Wu and Y. Li, *ACS Catal.*, 2018, **8**, 7879–7888.
33 C. Tang, T. Bao, S. Li, X. Li, H. Rao, P. She and J. Qin, *Adv. Funct. Mater.*, 2025, **35**, 2415280.
34 J. Luo, X. Wei, Y. Qiao, C. Wu, L. Li, L. Chen and J. Shi, *Adv. Mater.*, 2023, **35**, 2210110.
35 C. Yuan, H. Yin, J. Li, Y. Zhang, H. Chen, D. Xiao, Q. Wang, Y. Zhang and Q.-K. Xue, *Nat. Commun.*, 2025, **16**, 6607.
36 T. Guo, R. Dang, A. Zheng, S. Wang, X. Dong, Z. Xiong, Z. Chen, Z. Hu, W. Chen and C. Wang, *Green Chem.*, 2025, **27**, 1157–1168.
37 Z. Zou, Y. Wang, T. Zhang, J. Lu, V. Turkevich, Y. Yu, J. Xu, H. Lin, Y. Li and L. Wang, *Chem. Eng. J.*, 2025, **520**, 165595.
38 Y. Liu, J. Wei, Z. Yang, L. Zheng, J. Zhao, Z. Song, Y. Zhou, J. Cheng, J. Meng, Z. Geng and J. Zeng, *Nat. Commun.*, 2024, **15**, 3619.
39 R. Chahal, R. Rathee, S. Dahiya, R. Punia, A. S. Maan, K. Singh, R. Tripathi, M. A. Manthrammel, M. Shkir and A. Ohlan, *Chem. Eng. J.*, 2025, **520**, 165715.
40 X. Li, G. Zhang, N. Li, Q. Xu, H. Li, J. Lu and D. Chen, *Nano Energy*, 2024, **126**, 109671.
41 J. Fan, L. Shi, H. Ge, J. Liu, X. Deng, Z. Li and Q. Liang, *Adv. Funct. Mater.*, 2025, **35**, 2412078.
42 F. Xu, L. Zheng, J. Zhang, Y. He, H. Cao, X. Zheng, H. García and J. Yu, *Nat. Catal.*, 2026, **9**, 73–86.
43 P. Zhou, I. A. Navid, Y. Ma, Y. Xiao, P. Wang, Z. Ye, B. Zhou, K. Sun and Z. Mi, *Nature*, 2023, **613**, 66–70.
44 B. Chen, Y. Wang, S. Shen, W. Zhong, H. Lu and Y. Pan, *Small Methods*, 2024, **8**, 2301598.
45 J. Zhao, Y. Wang, H. Liu, R. Zhang, W. Jia, J. Zhang, Y. Sun and L. Peng, *ACS Catal.*, 2025, **15**, 3464–3474.

46 Y. Wang, H. Liu, T. Lv, W. Jia, R. Zhang, L. Peng and J. Zhang, *Adv. Funct. Mater.*, 2024, **35**, 2415842.
47 Z. Xue, B. Zhang, Q. Guo, Y. Wang, Q. Li, K. Yang and S. Qiao, *Adv. Mater.*, 2025, **37**, e10201.
48 Y. Deng, W. Liu, R. Xu, R. Gao, N. Huang, Y. Zheng, Y. Huang, H. Li, X. Kong and L. Ye, *Angew. Chem., Int. Ed.*, 2024, **63**, e202319216.
49 W. Xue, Y. Liu, X. Ma, J. Ye, X. Bai, J. Zhao and B. Liu, *ACS Catal.*, 2025, **15**, 9621–9632.
50 X. Cheng, Q. Sun, G. Zhang, W. Xing, Z.-A. Lan, S. Wang and Z. Pan, *ACS Catal.*, 2025, **15**, 13167–13178.
51 Y. Fan, Z. Hu, X. Hao and Z. Jin, *Carbon*, 2024, **228**, 119418.
52 H. Ding, R. Shen, K. Huang, C. Huang, G. Liang, P. Zhang and X. Li, *Adv. Funct. Mater.*, 2024, **34**, 2400065.
53 X. Ma, Z. Wu, Z. Zhou, S. Lu and Z. Jin, *Appl. Catal., B*, 2025, **278**, 125614.
54 H. L. He, L. L. Zhang, H. Zhou, Y. Nie, H. Wang, B. Tang, H. Li, T. Ma and H. Zhang, *Adv. Energy Mater.*, 2024, **15**, 2403168.